Asian Journal of Chemistry; Vol. 34, No. 12 (2022), 3286-3292

ASIAN JOURNAL OF CHEMISTRY

https://doi.org/10.14233/ajchem.2022.23980

Antibacterial, Anticancer, Catalytic and Antioxidant Activities of Green Synthesized Silver Nanoparticles Derived from *Alternanthera sessilis* Leaf Extract

B. Hari Babu[1,*] and G. Vijaya Lakshmi[2]

[1]Department of Chemistry, M.A.L.D. Government Degree College (Affiliated to Palamuru University), Gadwal-509125, India
[2]Department of Chemistry, University College for Women, Affiliated to Osmania University, Koti, Hyderabad-500009, India

*Corresponding author: E-mail: harirk95@gmail.com

Received: 24 June 2022; *Accepted*: 17 October 2022; *Published online*: 25 November 2022; AJC-21058

The current study evaluates the biogenesis of silver nanoparticles (Ag NPs) utilizing an aqueous extract of *Alternanthera sessilis* (Linn.) leaf. Biological nanoparticle production has recently gained appeal due to its eco-friendliness, simplicity, cost-effectiveness, non-hazardous nature and difficult circumstances. Aqueous extract of *Alternanthera sessilis* leaf contains terpenoids, carbohydrates and flavonoids to convert metal ions into metal and so stabilize the resultant nanoparticles. The UV-visible spectrophotometer obtained a distinctive peak at 420 nm, the XRD validated the crystalline FCC nature of biogenic Ag NPs and the FTIR and zeta-potential (± 14) tests revealed that phyto-chemicals were responsible for reduction and stabilization of Ag NPs. TEM examination revealed a spherical form and size of about 24 nm. The biogenic Ag NPs displayed intriguing dose-dependent antioxidant activity, with an EC_{50} percent of 69.9g/mL and a maximum activity of 66.36 at 150 µg/mL against DPPH, as well as considerable catalytic activity against Eosin-Y red dye, 84% of Eosin-Y dye destroyed after 60 min. Furthermore, the experiments demonstrated that Ag NPs were more effective against Gram-negative bacteria than Gram-positive bacteria and also show the anticancer activity against Hela cells and breast cancer cell line (MCF-7).The anticancer activity is more potent in higher concentrations.

Keywords: Silver nanoparticles, *Alternanthera sessilis* (Linn.), Biological activities, Catalytic activity, Phytochemicals.

INTRODUCTION

Biological synthetic approaches for silver nanoparticles provide new opportunities for synthesizing by utilizing natural reducing and stabilizing agents. It is a less expensive and eco-friendly alternative to chemical and physical procedures, as it does not require any energy or toxic ingredients [1]. Biosynthesis of nanoparticles is a bottomup strategy that employs simple unicellular to complex multicellular biological entities such as bacteria, fungus, actinomycetes and yeast, algae and plant materials [2,3].

When substances are produced at the nanoscale level, their properties vary as a result of specific factors such as reduced size, distribution and shape compared to their bulk counterparts. Nanoparticles have a higher surface-to-volume ratio due to their small size. The surface area of nanoparticles is critical for their catalytic activity as well as other associated qualities such as antibacterial capabilities [4].

Nanoparticles of various metals such as silver, gold, platinum, copper, zinc, titanium and magnesium have attracted a lot of attention for biomedical applications due to their multifunctional theranostics properties [5]. Because of its outstanding antibacterial and therapeutic properties, silver has been widely used for the treatment and control of several disorders since ancient times. Silver ions and silver-based compounds are well known for their excellent microbial killing power [6,7]. Silver nanoparticles are important in nanomedicine because of their appealing physico-chemical properties and biological features, such as high antimicrobial efficacy and low toxicity and wide range of bactericidal properties [8], anticancer properties and other therapeutic abilities and distinctive ability to form diverse nanostructures [9].

Another intriguing property of silver nanoparticles is their catalytic activity in the presence of sodium borohydrate, which is a novel and fast method of removing pollutants of from water contaminated by direct release of untreated industrial

effluents from the plastics, paints and textile industries. Specifically, organic dyes derived from these industries are known to be mutagenic, carcinogenic and environmentally hazardous [10].

The commonly used chemical and physical processes for synthesizing silver nanoparticles can be replaced by plant-based methods. The processes that are routinely employed to create silver nanoparticles chemically and physically can be replaced with plant-based methods [11,12]. Plants are bequeathed with abundant active constituents' phenols, alkaloids, flavonoids, terpenoids, saponins, tannins, polysaccharides, polyphenols vitamins, *etc*. These constituents were effectively reduced and stabilized the nanoparticles [1].

Alternanthera sessilis (Linn.) R.Br. is a perennial herb in the *Amaranthaceae* family found throughout India with a short petiole, simple leaves and white flowers. It is also known as sessile joy weed or dwarf copperleaf in English. The plant has traditionally been used to treat skin conditions, haemorrhoids, liver and spleen problems, asthma, wound healing and as an antidiabetic agents [13,14]. The *Alternanthera sessilis* (Linn.) leaf extract's bioactive components could be employed to make prepare nanoparticles. The effect of several parameters (time interval, temperature, concentration, *etc*.) on the synthesis of silver nanoparticles was examined using *Alteranthera sessilis* (Linn.) leaf extract. The synthesized silver nanoparticles were evaluated for its antibacterial effectiveness against *Alcaligenes faecalis*, *Escherichia coli*, *Staphylococcus aureus*, *Serratia marcescens* and also its degradation potential ability against Eosin-Y dye.

EXPERIMENTAL

The chemicals *viz*. silver nitrate, sodium borohydride, Eosin-Y dye and analytical grade solvents were obtained from Merck. Culture media was obtained from Hi-media Company and bacterial inoculums from Department of Microbiology, Osmania University, Hyderabad, India. All the glassware used in the present work was sterilized in hot air oven before use. Fresh leaves of *A. sessilis* were collected from Gadwal area, India. The plant specimen was identified and authenticated by Department of Botany, Osmania University, Hyderabad, India.

Preparation of *A. sessilis* (Linn.) leaf extracts: Fresh *A. sessilis* leaves were washed many times with running tap water to remove dust before being chopped into small chunks and dried for two weeks in shade. The dried leaves were pulverized and 10 g of powder were mixed into 300 mL of double distilled water, heated for 30 min on a magnetic stirrer at 40 ºC and filtered through Whatman No. 1 filter paper. The filtration procedure was repeated and the resulting filtrate was preserved at 4 ºC for further experiments. The filtrate obtained was then subjected to phytochemical analysis to detect the presence of secondary metabolites for bioreduction and stability of silver nanoparticles [13].

Biogenesis of silver nanoparticles: Aqueous solution (1 mM) of silver nitrate was prepared and utilized for biogenesis of silver nanoparticles. *A. sessilis* leaf extract (10 mL) was mixed with 90 mL of 1 mM silver nitrate and heated on a magnetic stirrer at 40 ºC for 30 min. The primary detection of synthesized silver nanoparticles in the reaction mixture was established by observing the colour change from green to dark brown. The reaction mixture was then centrifuged for 15 min at 4000 rpm. The collected residue was rinsed thrice with double distilled water and centrifuged again. The resulting residue was dried in an oven at 100 ºC for 24 h and the powder was kept for further investigations [15].

Characterization: The absorption was recorded by UV-visible spectrophotometer 2550 (Shimadzu, Japan) at a resolution of 1 nm in the wavelength range of 200-600 nm. A Fourier transform infrared spectrometer (FTIR spectrometer vector 22, Bruker, Germany) was used to determine the functional group of the biosynthesized silver nanoparticles utilizing the dried powder of synthesized AgNPs in the spectral region of 4000-400 cm^{-1}. The XRD patterns of the biosynthesized AgNPs were analyzed by using XPert PRO diffractometer (Holland) with a detector voltage of 45 kV and a current of 40 mA using Cu$K\alpha$ radiation. The recorded range of 2θ was 10-80º with a scanning speed of 4º min^{-1}.

The structural morphology of biosynthesized AgNPs had been recorded by scanning electron microscopy (TM-1000, Hitachi, Japan). The film obtained from the sample was fixed on a carbon-coated grid. The instrument was equipped with an energy dispersive spectrum (EDS) to ensure the presence of silver metal. The morphology of biosynthesized AgNPs was determined by TEM observation using a transmission electron microscopy (JEM-1230, JEOL, Japan). In brief, the sample was prepared with the copper coated grid for 24 h at room temperature to make a film of the sample. The excess liquid was discarded and kept in a grid box sequentially.

Catalysis of Eosin Y with silver nanoparticles: In brief, 50 mg of AgNPs were mixed with $NaBH_4$ solution (1 mL, 100 mM) and 75 mL of Eosin Y dye solution (10 mg/L) in a 200 mL reaction vessel. At 10 min of periodic time intervals, 5 mL of aliquots were collected by filtration and analyzed using the major absorption peak at 533 nm [16]. Before subjecting to spectral analysis, the suspensions were stirred magnetically for 1 h to ensure the adsorption-desorption equilibrium of the working solution. The rate of degradation of Eosin Y dye solution was estimated using the following equation:

$$\text{Degradation rate } (\%) = \frac{C_o - C}{C_o} \times 100 \quad (1)$$

where C_o is the absorption intensity of initial dye solution and C is the main absorption peak intensity of dye.

Antioxidant activity: 2,2′-Diphenyl-1-picrylhydrazyl (DPPH) scavenging potential of the biosynthesized silver nanoparticles from *A. sessilis* leaf aqueous extract was determined using the method of Mensor *et al.* [17]. Different concentrations (50, 75, 100, 125 and 150 µg/mL) of silver nanoparticles and the standard (ascorbic acid) were taken in different test tubes. Thereafter, 1 mL of freshly prepared DPPH (0.3 mM) was added to each test tube and vortexed thoroughly. Finally, the solution was incubated in dark place for 30 min. For control, 2 mL of methanol was added instead of silver nanoparticles and run simultaneously with the test.

The percentage DPPH radical scavenging activity of the silver nanoparticles was calculated using eqn. 2:

$$\text{DPPH radical scavenging activity (\%)} = \frac{A_c - A_s}{A_c} \times 100 \quad (2)$$

where A_c is the control absorbance of DPPH radical + methanol; A_s is the sample absorbance of DPPH radical + sample AgNPs/ ascorbic acid.

Antimicrobial sensitivity: The antimicrobial activity of silver nanoparticles was studied against two Gram-negative bacterial strains *Pseudomonas aeruginosa* (MTCC 441) and *Escherichia coli* (MTCC 442), two Gram-positive bacterial strains *Klebsiella pneumoniae* (MTCC 109) and *Staphylococcus aureus* (MTCC 96) using the agar well diffusion method. The bacterial cultures were adjusted to 0.5 McFarland turbidity standards before being injected on a 9 cm Muller-Hinton agar plate. Each of the standardized test organisms (1 mL) was swabbed on plate before drilling four wells (6 mm in diameter) with a sterile cork borer. Aliquots of *A. sessilis* AgNPs dilutions (25, 50, 75 and 100 µg/mL) were loaded to each well in the culture plates which had been previously been loaded with the test organisms. Following that, the plates were incubated at 37 ºC for 24 h for bacteria, while commercial antibiotic ampicillin (10 µg/mL) was used as a positive control [18]. The antimicrobial activity biogenic nanoparticles were assessed by measuring the zone of inhibition surrounding each well (excluding the diameter of the well). The experiments were carried out in triplicate.

Anticancer activity: To explore the anticancer activity of biosynthesized AgNPs, an MTT assay was employed to evaluate HeLa cells lines and breast cancer cell line (MCF-7). Both were cultured in DMEM supplemented with 10% FBS complete medium in a humidified atmosphere incubator containing 5% CO_2 at 37 ºC. The cells were plated into 96-well flat-bottomed plates at a density of 10000 cells per well and cultured for 24 h. Then, the growth medium was replaced with fresh DMEM medium containing different concentrations of AgNPs. After incubation for another 24 h, the relatively viable cells were determined by MTS. The absorbance was measured at 490 nm using a microplate reader (Molecular Devices, USA). Non treated cells in DMEM medium were used as a control.

RESULTS AND DISCUSSION

UV-visible studies: UV-vis spectrophotometric analysis of AgNPs with sizes ranging from 10 to 100 nm often yields absorbance peaks (max) ranging from 400 to 500 nm due to surface plasmon resonance (SPR) [19]. Fig. 1 displays the absorbance peaks of *A. sessilis* aqueous extract and precursor solution as well as the characteristic absorbance peak of the biogenic-AgNPs produced in this study around 420 nm [20]. This validates the biosynthesis of AgNPs by *A. sessilis* leaf aqueous extract.

Effect of pH on biogenesis of AgNPs: The significance of pH during nanoparticle production influences not only particle size but also particle shape. Yang & Li [21] demonstrated that the morphology of nanoparticles prepared at lower pH levels was less regular and tended to agglomerate. The nanoparticles develop cluster distribution at the colloidal stage

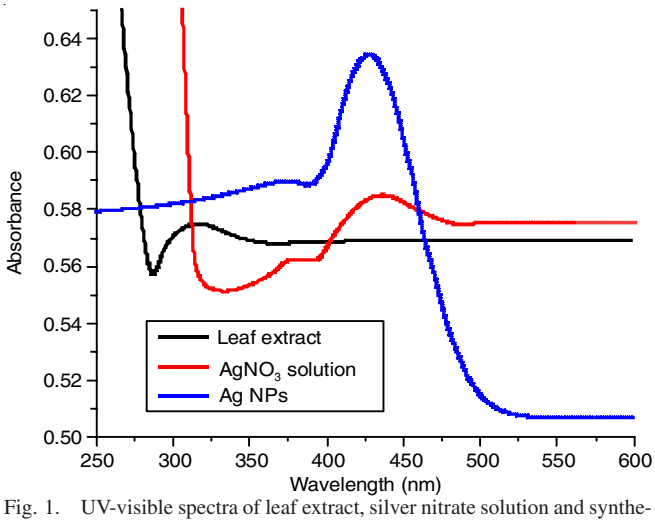

Fig. 1. UV-visible spectra of leaf extract, silver nitrate solution and synthesized biogenic Ag NPs

at alkaline pH, inhibiting aggregation [22]. While an alkaline pH improves the probability of available ligands in the reaction medium, this promoted nucleation and the creation of nanoparticles. Similar to the earlier work, the prominent peak at 420 nm (Fig. 2a) was obtained in an alkaline solution (pH = 8) in the current experiment. The existence of a pronounced peak suggested that spherical silver nanoparticles were produced [23].

Effect of precursor concentration: At low precursor/ metal ion concentrations, reducing agents in aqueous solution spontaneously reduce metal ions to metal atoms, which then adhere to the surface of preformed AgNPs and drive secondary reduction, resulting in larger nanoparticles and metal ion reduction is significantly reduced at higher metal ion concentrations due to a scarcity of reducing agents, resulting in the formation of fewer nanoparticles [24]. A stronger peak at 420 nm was exhibited due to 1 mM precursor concentration (Fig. 2b), which is agreement with the previous findings [25]. While low doses such as 0.01, 0.05 mM exhibited the weak peaks, increasing the concentration to 2 mM resulted in a blue shift along with a drop in peak intensity [25].

Effect of reaction incubation time: In this study, synthesis of silver nanoparticles at various time intervals (20-50 min) was studied. After reaction for 20 min, the AgNPs showed a UV-vis absorption peak, the intensity of the peak increased as the reaction time increased, which indicated the continued reduction of the silver ions. The increase of the absorbance with the reaction time indicates that the concentration of AgNPs increases (Fig. 2c). When the reaction time reached 50 min, the absorbance was considerably increased and no significant change in λ_{max} (420 nm) as compared to 40 min reaction time was observed.

Effect of temperature: The behaviour of silver nanoparticles over a temperature range was examined for the biogenesis of AgNPs at different temperatures ranging from 20 to 50 °C. As the reaction temperature rises, so does the reduction rate and most metal ions were consumed in the production of nuclei, preventing the secondary reduction process from taking place on the surface of the preformed nuclei [26]. In current study (Fig. 2d), when temperature rises (20-50 ºC), the creation

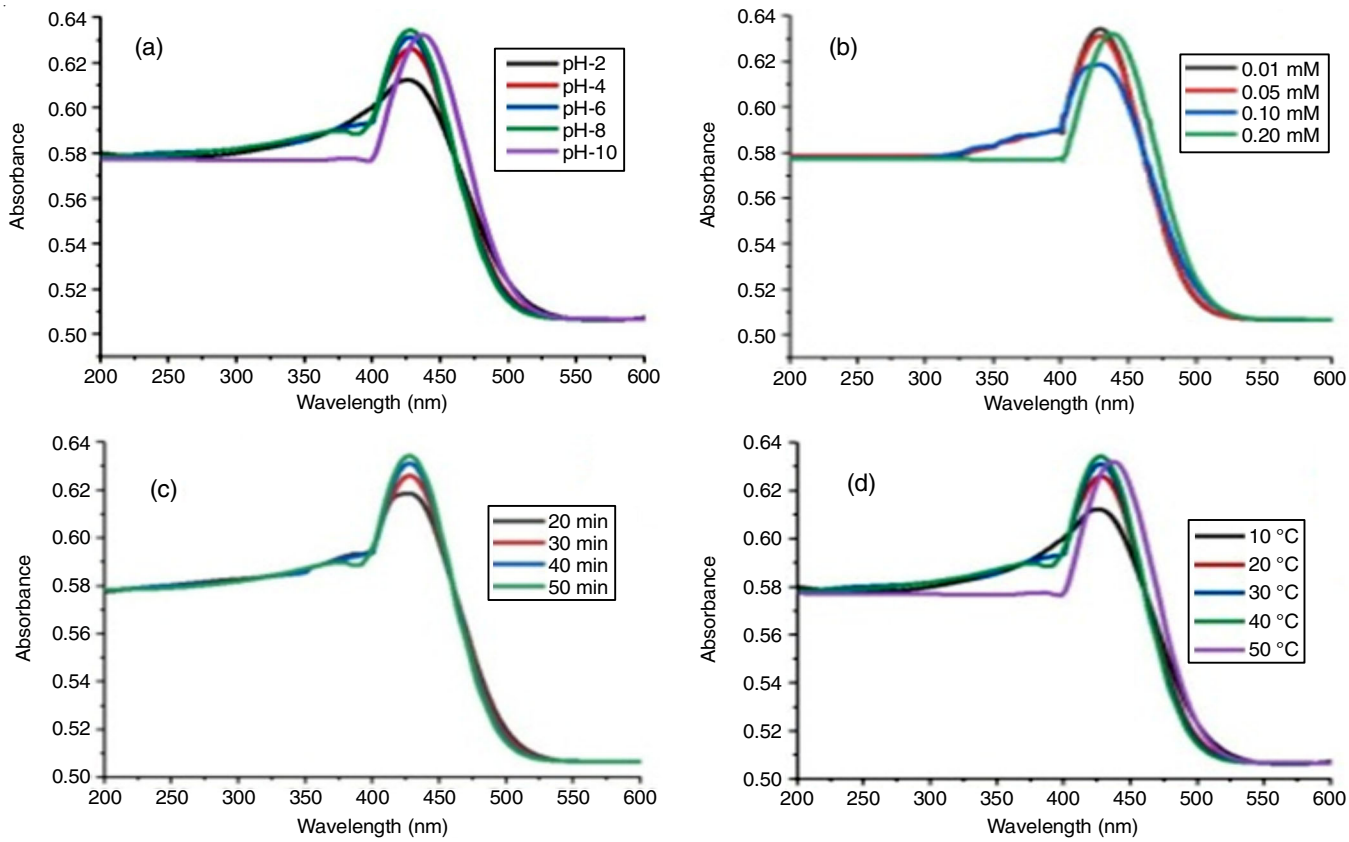

Fig. 2. (a) Effect of pH, (b) effect of precursor concentration, (c) effect of time, and (d) effect of temperature on synthesized biogenic Ag NPs

of tiny and highly mono dispersed nanoparticles increases, as evidenced by the broader and smaller peak becoming sharper and more intense [27].

FTIR studies: In the FTIR spectra (Fig. 3), the peak at 3378 cm^{-1} indicates the presence of –OH group stretching in acids, alcohols and phenols, the peak at 1640 cm^{-1} indicates the presence of >C=O group stretching, the peak at 1392 cm^{-1} corresponds to C-O stretching, while the weak peaks between 950.61 cm^{-1} and 656 cm^{-1} are associated with halo compound stretching [28]. As a result, these findings revealed the formation of AgNPs associated with metabolites such as terpenoids, which contain functional groups such as alcohols, phenols, aldehydes, ketones, carboxylic acids, *etc*. According to Urnukhsaikhan *et al.* [29], bioentities could likely play a dual role in the synthesis and stabilization of silver nanoparticles in aqueous solution.

XRD studies: The XRD patterns of the biosynthesized *A. sessilis* AgNPs revealed four intense peaks at 38.6º, 43.1º, 64.34º and 77.56º, which correspond to the silver planes (111), (200), (220) and (311), respectively (Fig. 4). Standard silver data from JCPDS card No. 04-0783 [30] was used to confirm the results. The XRD pattern verified the crystalline character (FCC) of the produced AgNPs, which was previously reported [31]. The mean crystalline size (D) of AgNPs was calculated by using the Debye Scherrer's formula:

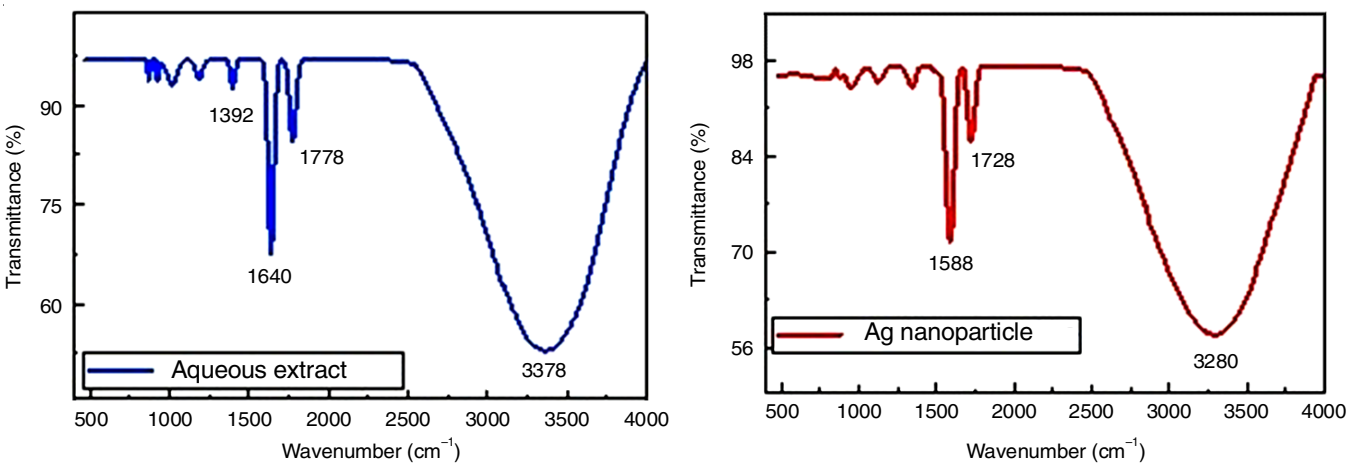

Fig. 3. FTIR of *A. sessilis* leaf extract and synthesized biogenic silver nanoparticles

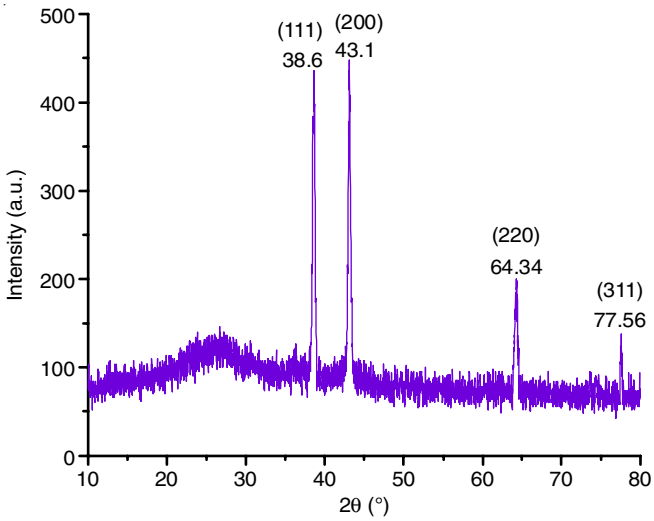

Fig. 4. XRD diffraction spectrum of synthesized biogenic Ag NPs

$$D = \frac{k\lambda}{\beta \cos\theta}$$

where D = particle diameter size, K = constant (equals 0.9 to 1), λ = wavelength of X-ray (0.1541 nm), β = full width at half maximum of the diffraction peak and θ = Bragg angle.

The mean crystalline size (D) of the biosynthesized AgNPs was estimated at 24.133 nm, which was very closely related to the TEM results.

Zeta potential: The zeta potential of nanoparticles in dry powder is larger than or less than 30 mV, indicating good stability [32]. A high negative value causes repulsion between like charged particles in suspension and thus preventing the aggregation [33]. According to present findings, the zeta potential of biosynthesized Ag NP was ± 14 on average. Fig. 5 depicted the zeta potential values of AgNPs indicating that silver nanoparticles generated are substantially monodisperse.

Morphological studies: The surface morphology of biosynthesized AgNPs was studied using scanning electron microscopy (SEM) technique. According to surface morphology studies, the size of AgNPs ranged between 0.04 and 8.733 µm. Fig. 6 shows the presence of AgNPs with irregular shapes and some large granular particles up to 8.733 µm in size, which could be attributed to particle aggregation [34].

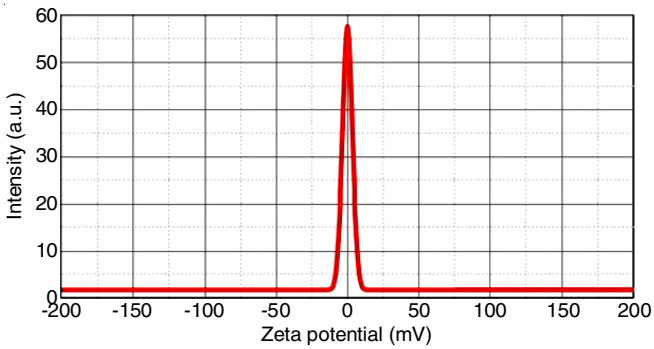

Fig. 5. Zeta-potential plot of synthesized biogenic Ag NPs

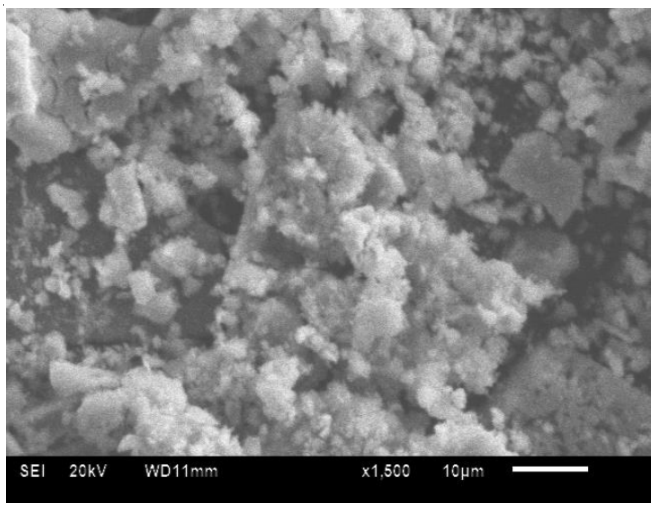

Fig. 6. SEM images of synthesized biogenic Ag NPs

The HRTEM micrographs (Fig. 7a) shows the topology and size of biosynthesized AgNPs, which exhibited heterogeneous and polydispersed properties. The produced AgNPs that were predominantly spherical in form and had an average diameter of 24 nm (Fig. 7b). These anisotropic geometries were most likely caused by reducing and capping phytochemicals, which not only provided thermodynamic stability but also defined nanoparticle bioactivities [35]. The fringe spacing of the clear lattice fringes in the HRTEM image was 0.28 nm (Fig. 7a), which corresponds to the (220) planes of silver. The crystalline character of AgNPs was verified by the typical selected-area

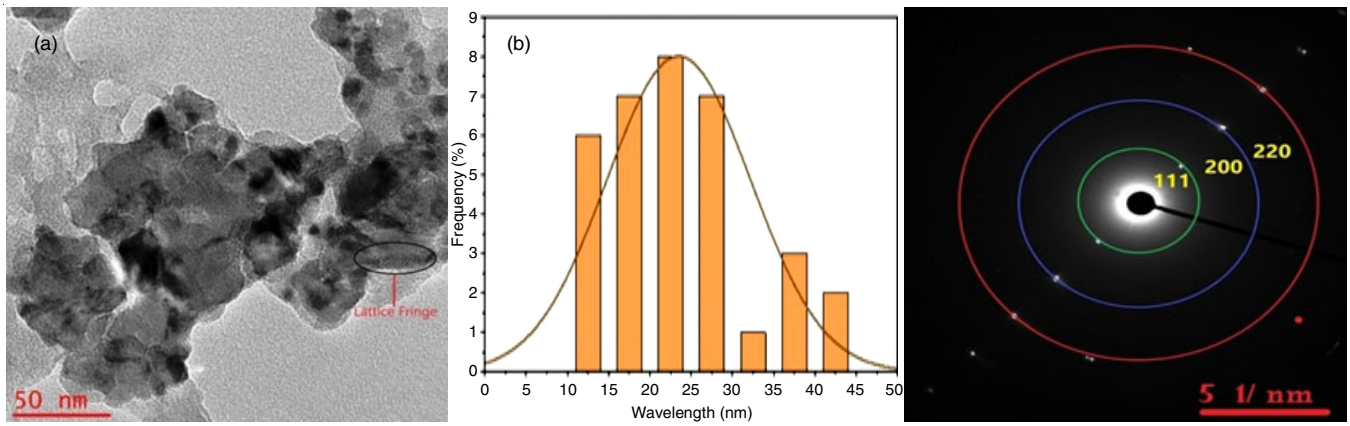

Fig. 7. (a) TEM image of Ag NPs, (b) particle size distribution of Ag NPs, (c) SAED pattern of Ag NPs

TABLE-1
SCAVENGING ACTIVITIES OF *A. sessilis* MEDIATED Ag NPs and ASCORBIC ACID AS STANDARD AGAINST DPPH ASSAY

Volume of DPPH (mL)	Concentration (µg/mL)		Scavenging activity (%)		IC_{50} values	
	Ag NPs	Ascorbic acid	Ag NPs	Ascorbic acid	Ag NPs	Ascorbic acid
3	50	50	13.66	10.27		
3	75	75	23.85	20.23		
3	100	100	46.25	36.78	78.73	67.49
3	125	125	54.95	44.34		
3	150	150	80.6	66.36		

diffraction (SAED) patterns, as shown in Fig. 7c, where the circular rings correspond to the (111), (200) and (220) planes [36].

Degradation studies: The catalytic activity of biogenic AgNPs against Eosin Y dye solution in the presence of sodium borohydride solution was studied using a UV-visible spectrometer in the 400-800 nmrange. Fig. 8a depicts the UV-Vis absorption spectra of the catalytic degradation of Eosin Y dye solution with AgNPs in the presence of $NaBH_4$ solution. The strength of the absorption peak at 533 nm declines significantly with time and 84% of Eosin Y decompose after 60 min (Fig. 8c). There was no substantial degradation observed in blank tests (without the catalyst) showing that the degradation was not effective by the catalyst. The decline in Eosin Y dye follows first-order kinetics [37]. The linear plot of $\ln(C_o/C_t)$ *vs*. reduction time revealed that the rate constant of (reduction of Eosin Y) pseudo-first-order reaction was 0.00648 s^{-1}.

Antioxidant activity: The AgNPs derived from the aqueous extract of *A. sessilis* were potential free radical scavengers with dose-dependent inhibitory activity at different concentrations of AgNPs (50, 75, 100, 125 and 150 µg/mL) reduced DPPH by 10.34, 20.73, 36.38, 44.34 and 66.36%, respectively (Table-1). These activities, however, are lower than those of ascorbic acid (standard).

Antibacterial activity: The antibacterial activity of silver nanoparticles was found to be dose dependent against pathogenic two Gram-negative bacterial strains of *Pseudomonas aeruginosa* (MTCC 441) and *Escherichia coli* (MTCC 442), two Gram-positive bacterial strains *Klebsiella pneumoniae* (MTCC 109) and *Staphylococcus aureus* (MTCC 96) using the well diffusion method. The antibacterial activity showed that biosynthesized AgNPs had efficient antibacterial activity against both Gram-negative *E. coli, Pseudomonas aeruginosa* and Gram-positive *Klebsiella pneumoniae* and *Staphylococcus aureus* bacterial strains. The inhibition zone of AgNPs, against *E. coli*, P. *aeruginosa, K. pneumoniae* and *S. aureus* were 12.782, 11.024, 8.06 and 7.98 mm respectively at 100 µg/mL concentration. Gram-negative strains were more sensitive to biosynthesized AgNPs due to their distinct outer layer and single peptidoglycan layer, whereas Gram-positive bacteria had a thick peptidoglycan layer, were more resistant to environmental conditions and had a strong chitinous membrane layer for protection [38]. In Table-2, the antibacterial activity of AgNPs (50 µg/mL) was compared to a positive control (ampicillin 10 µg/mL) against all four pathogenic bacterial strains.

TABLE-2
COMPARATIVE STATEMENT OF ZOI (mm) OF Ag NPs AND AMPICILLIN (POSITIVE CONTROL) AGAINST PATHOGENIC BACTERIAL STAINS

Conc. (µg/mL)	Diameter of zone of inhibition (mm)			
	E. coli	*P. aeruginosa*	*K. pneumoniae*	*S. aureus*
25	5.14	3.4933	2.719	2.073
50	6.15	5.2066	3.1513	3.543
75	10.74	9.2356	5.1133	5.3264
100	12.7822	11.024	8.0616	7.985
Ampicillin	20.4	18.25	16.08	16.86

Anticancer activity: The anticancer activity of biosynthesized AgNPs from *Alternanthera sessilis* leaf extract was studied at various doses. The anticancer activity is more potent in higher concentrations. Around 85.69 and 76.82% of cancer cells were killed of HeLa cells & breast cancer cell line (MCF-7) with 300 µM AgNPs. Table-3 shows the HeLa cells and breast cancer cell line proliferation inhibitory activity data of the *Alternanthera sessilis* mediated silver nanoparticles.

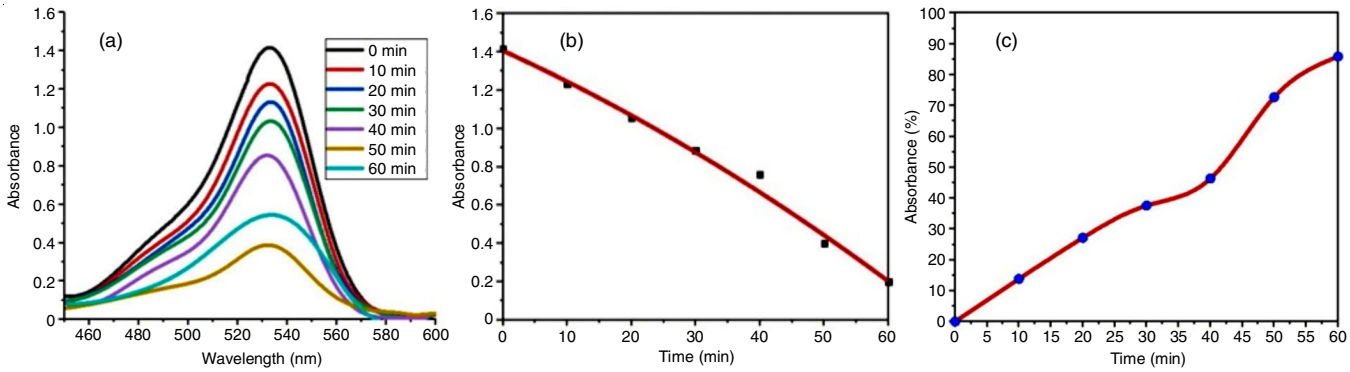

Fig. 8. (a) Plot of catalytic activity of Ag NPs, (b) reduction of Eosin Y dye in presence of Ag NPs, (c) % of reduction of Eosin Y dye by Ag NPs

TABLE-3
HeLa CELLS & BREAST CANCER CELL LINE
INHIBITORY ACTIVITY OF *Alternanthera sessilis*
MEDIATED SILVER NANOPARTICLES

Ag NPs (µM)	Inhibition (%)	
	HeLa cells	Breast cancer cell line MCF-7
10	0.75 ± 0.008	0.48 ± 0.032
25	5.68 ± 0.06	11.72 ± 0.076
50	37.82 ± 0.28	28.37 ± 0.26
100	51.41 ± 0.064	50.06 ± 0.21
200	68.29 ± 0.66	59.27 ± 1.04
300	85.69 ± 1.98	76.82 ± 1.79

Conclusion

A green synthetic approach was used to successfully synthesized AgNPs using *Alternanthera sessilis* extract. The FCC crystal structure of AgNPs has been validated using XRD data. The TEM and SAED results matched with the XRD data quite well. According to FTIR and zeta-potential examinations, the terpenoids and alkaloids in the aqueous extract of *A. sessilis* leaves acted as reducing and capping agents to stabilize the biosynthesized AgNPs. Biogenic AgNPs also displayed anti-oxidant, antibacterial and catalytic activity against DPPH, two Gram-positive and two Gram-negative bacteria and Eosin-Y (EY) dye, respectively.

CONFLICT OF INTEREST

The authors declare that there is no conflict of interests regarding the publication of this article.

REFERENCES

1. S. Patil and R. Chandrasekaran, *J. Genet. Eng. Biotechnol.*, **18**, 67 (2020); https://doi.org/10.1186/s43141-020-00081-3
2. M. Shah, D. Fawcett, S. Sharma, S.K. Tripathy and G.E.J. Poinern, *Materials*, **8**, 7278 (2015); https://doi.org/10.3390/ma8115377
3. S. Patil and R. Chandrasekaran, *J. Genet. Eng. Biotechnol.*, **18**, 67 (2020); https://doi.org/10.1186/s43141-020-00081-3
4. A. Albanese, P.S. Tang and W.C.W. Chan, *Ann. Rev. Biomed. Eng*., **14**, 1 (2012); https://doi.org/10.1146/annurev-bioeng-071811-150124
5. A. Mishra, S. Singla and A.K. Barui, Biogenic Nanoparticles for Cancer Theranostics, In: Micro and Nano Technologies, Elsevier, pp. 123-140 (2021); https://doi.org/10.1016/B978-0-12-821467-1.00011-2
6. R.M. Slawson, J.T. Trevors and H. Lee, *Arch. Microbiol.*, **158**, 398 (1992); https://doi.org/10.1007/BF00276299
7. G. Zhao and S.E. Stevens Jr., *Biometals*, **11**, 27 (1998); https://doi.org/10.1023/A:1009253223055
8. M.A. Khalil, G.M. El Maghraby, F.I. Sonbol, N.G. Allam, P.S. Ateya and S.S. Ali, *Front. Microbiol.*, **12**, 648560 (2021); https://doi.org/10.3389/fmicb.2021.648560
9. A. Almatroudi, *Open Life Sci.*, **15**, 819 (2020); https://doi.org/10.1515/biol-2020-0094
10. A. Roy and N. Bharadvaja, *Biomimetic Nanobiomater.*, **8**, 130 (2019); https://doi.org/10.1680/jbibn.18.00036
11. J. Singh, T. Dutta, K.-H. Kim, M. Rawat, P. Samddar and P. Kumar, *J. Nanobiotechnol.*, **16**, 84 (2018); https://doi.org/10.1186/s12951-018-0408-4
12. M. Ndikau, N.M. Noah, D.M. Andala and E. Masika, *Int. J. Anal. Chem.*, **2017**, 1 (2017); https://doi.org/10.1155/2017/8108504
13. R.K. Singla, V. Dhir, R. Madaan, D. Kumar, S. Singh Bola, M. Bansal, S. Kumar, A.K. Dubey, S. Singla and B. Shen, *Front. Pharmacol.*, **13**, 769111 (2022); https://doi.org/10.3389/fphar.2022.769111
14. L. Qian, W. Su, Y. Wang, M. Dang, W. Zhang and C. Wang, *Artif. Cells Nanomed. Biotechnol.*, **47**, 1173 (2019); https://doi.org/10.1080/21691401.2018.1549064
15. C.E. Escárcega-González, J.A. Garza-Cervantes, A. Vázquez-Rodríguez, L.Z. Montelongo-Peralta, M.T. Treviño-González, E. Díaz Barriga Castro, E.M. Saucedo-Salazar, R.M. Chávez Morales, D.I. Regalado-Soto, F.M. Treviño-González, J.L. Carrazco Rosales, R. Villalobos Cruz and J.R. Morones-Ramirez, *Int. J. Nanomedicine*, **13**, 2349 (2018); https://doi.org/10.2147/IJN.S160605
16. V.K. Vidhu and D. Philip, *Micron*, **56**, 54 (2014); https://doi.org/10.1016/j.micron.2013.10.006
17. L.L. Mensor, F.S. Menezes, G.G. Leitão, A.S. Reis, T.C. Santos, C.S. Coube and S.G. Leitão, *Phytother. Res.*, **15**, 127 (2001); https://doi.org/10.1002/ptr.687
18. A.K. Keshari, R. Srivastava, P. Singh, V.B. Yadav and G. Nath, *J. Ayurveda Integr. Med.*, **11**, 37 (2020); https://doi.org/10.1016/j.jaim.2017.11.003
19. M.S. Majoumouo, N.R.S. Sibuyi, M.B. Tincho, M. Mbekou, F.F. Boyom and M. Meyer, *Int. J. Nanomedicine*, **14**, 9031 (2019); https://doi.org/10.2147/IJN.S223447
20. Hemlata, P.R. Meena, A.P. Singh and K.K. Tejavath, *ACS Omega*, **5**, 5520 (2020); https://doi.org/10.1021/acsomega.0c00155.
21. N. Yang and W. Li, *Ind. Crops Prod.*, **48**, 81 (2013); https://doi.org/10.1016/j.indcrop.2013.04.001
22. L.B. Anigol, J.S. Charantimath and P.M. Gurubasavaraj, *Org. Med. Chem.*, **3**, 1 (2017); https://doi.org/10.19080/OMCIJ.2017.03.555622
23. M.S. Samuel, M. Ravikumar, A. John J., E. Selvarajan, H. Patel, P.S. Chander, J. Soundarya, S. Vuppala, R. Balaji and N. Chandrasekar, *Catalysts*, **12**, 459 (2022); https://doi.org/10.3390/catal12050459
24. S. Raj, R. Trivedi and V. Soni, *Surfaces*, **5**, 67 (2021); https://doi.org/10.3390/surfaces5010003
25. K. Gopinath, S. Gowri and A. Arumugam, *J. Nanostructure Chem.*, **3**, 68 (2013); https://doi.org/10.1186/2193-8865-3-68
26. S.M. Rakib-Uz-Zaman, E.H. Apu, M.N. Muntasir, S.A. Mowna, M.G. Khanom, S.S. Jahan, N. Akter, M.A.R. Khan, N.S. Shuborna, S.M. Shams and K. Khan, *Challenges*, **13**, 18 (2022); https://doi.org/10.3390/challe13010018
27. J.K. Patra and K. Baek, *J. Nanomater. Synth.*, **2014**, 417305 (2014); https://doi.org/10.1155/2014/417305
28. R. Mata, J.R. Nakkala and S.R. Sadras, *Colloids Surf. B Biointerfaces*, **128**, 276 (2015); https://doi.org/10.1016/j.colsurfb.2015.01.052
29. E. Urnukhsaikhan, B.E. Bold, A. Gunbileg, N. Sukhbaatar and T. Mishig-Ochir, *Sci. Rep.*, **11**, 21047 (2021); https://doi.org/10.1038/s41598-021-00520-2
30. L. Budama, B.A. Çakir, Ö. Topel and N. Hoda, *Chem. Eng. J.*, **228**, 489 (2013); https://doi.org/10.1016/j.cej.2013.05.018
31. K. Anandalakshmi, J. Venugobal and V. Ramasamy, *Appl. Nanosci.*, **6**, 399 (2016); https://doi.org/10.1007/s13204-015-0449-z
32. H. Padalia, P. Moteriya and S. Chanda, *Arab. J. Chem.*, **8**, 732 (2015); https://doi.org/10.1016/j.arabjc.2014.11.015
33. T.A. Jorge de Souza, L.R. Rosa Souza and L.P. Franchi, *Ecotoxicol. Environ. Saf.*, **171**, 691 (2019); https://doi.org/10.1016/j.ecoenv.2018.12.095
34. Y. Sun, B. Gates, B. Mayers and Y. Xia, *Nano Lett.*, **2**, 165 (2002); https://doi.org/10.1021/nl010093y
35. K. Mohan Kumar, M. Sinha, B.K. Mandal, A.R. Ghosh, K. Siva Kumar and P. Sreedhara Reddy, *Spectrochim. Acta A Mol. Biomol. Spectrosc.*, **91**, 228 (2012); https://doi.org/10.1016/j.saa.2012.02.001
36. M.J. Khan, K. Shameli, A.Q. Sazili, J. Selamat and S. Kumari, *Molecules*, **24**, 719 (2019); https://doi.org/10.3390/molecules24040719
37. R. Karthik, M. Govindasamy, S.M. Chen, P. Muthukrishnan, Y.H. Cheng, S. Padmavathy and A. Elangovan, *J. Photochem. Photobiol. B*, **170**, 164 (2017); https://doi.org/10.1016/j.jphotobiol.2017.03.018
38. S. Rajeshkumar, S. Menon, S. Venkat Kumar, M.M. Tambuwala, H.A. Bakshi, M. Mehta, S. Satija, G. Gupta, D.K. Chellappan, L. Thangavelu and K. Dua, *J. Photochem. Photobiol. B*, **197**, 111531 (2019); https://doi.org/10.1016/j.jphotobiol.2019.111531